Phosphate adsorption and desorption on two-stage synthesized amorphous-ZrO2/Mg–Fe layered double hydroxide composite

by Atin Nuryadin

Submission date: 22-Feb-2022 11:04AM (UTC+0700)
Submission ID: 1768052430
File name: 1-s2.0-S0254058421003424-main.pdf (8.35M)
Word count: 8447
Character count: 44218

Materials Chemistry and Physics 266 (2021) 124559

Contents lists available at ScienceDirect

Materials Chemistry and Physics

journal homepage: www.elsevier.com/locate/matchemphys

Phosphate adsorption and desorption on two-stage synthesized amorphous-ZrO_2/Mg–Fe layered double hydroxide composite

Atin Nuryadin [a,b], Tsuyoshi Imai [a,*], Ariyo Kanno [a], Koichi Yamamoto [a], Masahiko Sekine [a], Takaya Higuchi [a]

[a] Graduate School of Sciences and Technology for Innovation, Yamaguchi University, Yamaguchi, 755-8611, Japan
[b] Department of Physics Education, Mulawarman University, Samarinda, 75123, Indonesia

HIGHLIGHTS

- Am-ZrO_2/MgFe-LDH composites were prepared by a two-stage synthesis.
- Uncalcined composite with Zr/Fe of 1.5 exhibited optimal phosphate adsorption.
- The acidic solution was preferred for phosphate adsorption on the composite.
- Adsorption was not significantly affected by Cl^-, NO^{3-}, and SO_4^{2-} but considerably reduced by HCO_3^-.
- Desorption and regeneration cycles showed the potential of practical application.

GRAPHICAL ABSTRACT

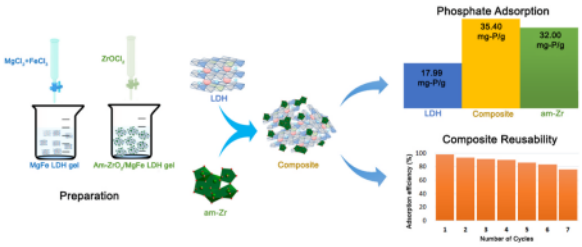

ARTICLE INFO

Keywords:
Layered double hydroxide
Amorphous zirconia
Composite
Phosphate
Adsorption

ABSTRACT

Although different treatment techniques have been developed to eliminate phosphorus contamination, including for wastewater treatment, treated water often fails to meet quality regulations. Amorphous-ZrO_2/Mg–Fe layered double hydroxide (LDH) composites with different molar ratios (Zr/Fe = 0.5–2) were prepared in two-stage synthesis by the combination of coprecipitation and hydrothermal methods. The requirement of high-temperature calcination in the LDH for phosphate adsorption could be eliminated by the synthesis of the composite. Moreover, the phosphate adsorption ability of the composite was higher than that of the individual LDH and amorphous-ZrO_2. The addition of ZrO_2 increased the phosphate adsorption ability of composite at low pH. The adsorption capacity was increased by decreasing the pH and increasing the temperature (from 290 to 324 K). The bicarbonate (HCO_3^-) was the most competitive anion for phosphate adsorption. The pseudo-second-order model provided the best description of the kinetic adsorption data. Furthermore, the adsorbed phosphate was easily desorbed by 1 N of NaOH solution. The results suggest that the amorphous-ZrO_2/Mg–Fe LDH composite is a promising material for phosphate removal and recovery from wastewater. Ongoing research will investigate the performance of the composite for real wastewater as well as the mechanism of phosphate adsorption on the composite surface.

Abbreviations: am-Zr, amorphous ZrO_2; DI, Deionized; LDH, layered double hydroxide; SEM, scanning electron microscopy; XRD, X-ray diffraction; FTIR, Fourier-transform infrared; MgFe-LDH, Mg-Fe layered double hydroxide; XPS, X-ray photoelectron spectroscopy.

* Corresponding author. Graduate School of Sciences and Technology for Innovation, Yamaguchi University, Tokiwadai 2-16-1, Ube, Yamaguchi, 755-8611, Japan.
E-mail address: imai@yamaguchi-u.ac.jp (T. Imai).

https://doi.org/10.1016/j.matchemphys.2021.124559
Received 22 April 2020; Received in revised form 25 December 2020; Accepted 28 March 2021
Available online 31 March 2021

1. Introduction

Phosphorus is imperative for the growth of all living things and is also used in food production [1]. However, excessive discharge of phosphorus in waterbodies often causes serious eutrophication problems, which leads to algal blooms, the disruption of aquatic ecosystems, and water quality deterioration [2]. Different treatment techniques have been developed to eliminate phosphorus (usually existing as phosphate in water) contamination, including biological and chemical methods, which have been widely used in wastewater treatment [3]. However, these methods have some limitations, such as the high cost of neutralizing products and handling the produced sludge for chemical methods [4], and inefficient elimination of trace levels of phosphate for biological methods [5]. Moreover, the resultant treated water often fails to meet the strict regulatory quality standard for phosphorus, which has recently become more stringent for wastewater treatment in some countries [6]. For example, the standard has been revised from 1.0 to 0.5 mg-P L^{-1} in China, and from 2.0 to 0.2 mg-P L^{-1} in some areas of Korea [7]. The concentration of phosphorus must be maintained as low as possible—even in waterbodies that are assessed as having a 'good' environmental condition—in order to conserve the water environment for the next generation, especially considering the difficulty of restoring eutrophic waterbodies.

Phosphate rock deposits are a non-renewable resource and experts estimate that reserves will only last until 2170 given the present usage and population growth rate [8]. Hence, the recovery and reuse of phosphorus offer the best strategies to meet the future phosphorus demand. Accordingly, adsorption represents a fascinating separation technique for phosphate from water because of the possibility of phosphorus recovery [5]. Moreover, this approach has many advantages, such as efficient, easy operating conditions, low sludge production, and the possibility of regenerating the adsorbent [9].

In recent decades, layered double hydroxide (LDH) materials have become very attractive as an inorganic anion adsorbent for deterging pollution in nature by anion exchange in the interlayer [10]. LDH is a layered material with hydroxide sheets, where a net positive charge is developed on the layer because trivalent cations partially substitute divalent cations. Unfortunately, the anion adsorption capacity of LDH is greatly influenced by the calcination process during the synthesis of LDH, whereby calcined LDH generally exhibits a higher adsorption capacity than uncalcined LDH [11,12]. Moreover, a high temperature, which requires additional energy, is needed both for the synthesis process and for the reuse of the material. In this study, a new composite of LDH is explored to eliminate the high temperature requirement during the synthesis process.

Many researchers have reported that the functionalization of zirconia (ZrO_2), an eco-friendly compound, markedly enhanced the phosphate adsorption ability of adsorbents [13–15]. This clearly relates to the fact that Zr(IV) is easily hydrolyzed to form tetranuclear ions or octanuclear species, thus producing a large number of hydroxyl ions and water molecules, which are involved in the exchange of ligands with phosphate ions in solution [16]. However, the application of pure zirconia is relatively high cost and requires a combination with other low-cost materials to make it more cost-effective. Since LDH is a bio-safe, low-cost, and environmentally friendly [17], combining zirconia with LDH is an attractive approach to lower the cost of zirconia application and produce an environment-friendly adsorbent. Moreover, enabling crystallization of zirconium (hydr)oxides on the LDH matrix can suppress the crystal growth resulting in nanosized particles, in which nanosized adsorbents are preferable because the crystal has a large number of adsorption sites.

Several studies have investigated the adsorption of phosphate by Zr modified LDH [18–20]. However, the type of modification of Zr to LDH remains unclear, as research is inconclusive over whether the Zr ions are distributed in the octahedral sites of the LDH layer, or if the growth of zirconium (hydr)oxides occurs separately and they form a composite with LDH. As reported by Tichit et al. (2002) and Velu et al. (1998), the mixing of solutions simultaneously containing LDH and Zr ions by a simple coprecipitation method resulted in the modification and incorporation of Zr into the LDH layers [21,22]. Although the uptake properties of phosphate by Zr modified Mg–Fe layered double hydroxides (MgFe-LDH), which was synthesized with the coprecipitation method, were studied by Chitrakar et al. (especially in seawater) [18], the effect of ZrO_2 on the adsorption stability of composites at low pH, as well as the adsorption kinetics and thermodynamics of composites, have not yet been explained.

In this study, a composite of amorphous-ZrO_2 (am-Zr) and MgFe-LDH was synthesized and its application for phosphate removal was systematically examined. The synthesis of the LDH and the addition of ZrO_2 to the LDH were performed separately into two stages to minimize the possibility of the LDH structural layer being modified by Zr ions. This new preparation method implies further investigation of phosphate adsorption characteristics of the composite, whereas a different preparation method could change the phosphate adsorption property of the same materials [19]. The characteristics of the composite at different Zr:Fe molar ratios were investigated, and their effect on the phosphate adsorption capacity was evaluated. The effect of pH and competing anions on phosphate adsorption to the composite were also examined. Furthermore, adsorption kinetics, isotherm, and thermodynamic models were applied to explain the properties of phosphate adsorption. Meanwhile, the reusability of the composite as phosphate adsorbent was also considered.

2. Experimental

2.1. Materials

All the chemicals used in this study ($FeCl_3{\cdot}6H_2O$, $MgCl_2{\cdot}6H_2O$, $ZrOCl_2{\cdot}8H_2O$, Na_2CO_3, K_2HPO_4, NaOH, and HCl) were analytical pure-grade reagents that acquired from Wako Pure Chemical Industries, Ltd., and used in their conditions as received without further purification. DI water was used for the preparation of the metal salt solutions.

2.2. Preparation of am-Zr/MgFe-LDH composites

The composites were synthesized in two stages by the combination of coprecipitation and hydrothermal methods. For the first stage, a solution containing $FeCl_3$ and $MgCl_2$ with an Mg^{2+}:Fe^{3+} molar ratio of 3:1 and a solution containing 1 M NaOH and 1 M Na_2CO_3 with a 3:1 vol ratio were added dropwise into 200 mL DI water under vigorous stirring. A pH of 10 was maintained under continuous stirring at room temperature (~298 K) for 30 min. The obtained gel was filtered and washed five times with DI water. For the second stage, the fresh LDH gel was dissolved into 500 mL of DI water. Different volumes of 1 M $ZrOCl_2$ were added to obtain various Zr contents in the composites (0.5, 1.0, 1.5, and 2.0 Zr:Fe molar ratios). Concurrently, a 25% NaOH solution was added to precipitate out the ZrO_2 until a pH of ~10 was reached, and was then stirred continuously for 30 min. The resultant precipitates were aged at 353 K for 24 h, whereby the gel was left in solution as a means of improving its crystallization. They were then separated and washed by DI water until the filtrate pH was ~7 before being dried in an oven at 353 K for 24 h. As a comparison, MgFe-LDH (hereafter LDH) and am-Zr were also synthesized separately under the same conditions as those used for the composite synthesis. Calcined samples were obtained by heating at 573 K for 3 h.

2.3. Characterization of am-Zr/MgFe-LDH composites

XRD patterns were recorded on Rigaku Ultima IV Protectus diffractometer using Cu-Kα radiation at 40 kV, with a scanning speed of 1°/min and 2θ angle ranging from 5° to 70°. The FTIR spectra of the samples were recorded on a Jasco FT/IR-4600 spectrophotometer within the

range of 4000 to 600 cm^{-1}. SEM images were collected by using a JEOL JSM-7600F field emission SEM at an accelerating voltage of 5 kV, in which the powdered samples were prepared on a carbon tape coated with a platinum film. The XPS spectra were obtained using a Thermo Scientific K-alpha X-ray photoelectron spectrometer.

2.4. Batch adsorption experiments

K_2HPO_4 (99.0%) was used to prepare a stock of phosphate solution, which was then diluted to the desired concentration using DI water to obtain the working solution. The solution was adjusted to the desired pH by using diluted HCl and NaOH. The sample (0.01 g) was shaken in 100 mL of the K_2HPO_4 solution (10 mg-P L^{-1}) at 140 rpm for 24 h. The supernatant was collected using a syringe and filtered through a 0.45 μm filter. The residual phosphate concentration was analyzed in triplicate using the ascorbic acid method and a Hitachi U-1800 UV/vis spectrophotometer at a wavelength of 880 nm. The phosphate adsorption capacity was calculated using Equation (1):

$$q_e = \frac{C_0 - C}{m} \times V \quad (1)$$

where q_e is the amount of adsorbed phosphate (mg-P g^{-1}), C_0 and C are the initial and residual phosphate concentrations (mg L^{-1}), respectively, m is the weight of the adsorbent (g), and V is the volume of the solution (L).

The effects of pH and competing anions on the adsorption capacity were investigated by shaking 0.01 g of sample in 100 mL of 3 mg-P L^{-1} phosphate solution at different pH (2–10) and concentrations (0.005 M and 0.01 M) of anions (Cl^-, NO_3^-, SO_4^{2-}, and HCO_3^-), respectively. The adsorption kinetics was investigated by shaking a 0.01 g sample in 100 mL of 10 mg-P L^{-1} phosphate solution. At various intervals between 0.5 h and 36 h, supernatants were collected for the determination of their phosphate concentration. The adsorption thermodynamics and adsorption isotherm were studied by different initial phosphate concentration (1–50 mg L^{-1}) at three different temperatures (290, 307, and 324 K) for 24 h.

2.5. Desorption experiments

The desorption ability of the adsorbent was investigated using NaOH (0.01, 0.1, 1, and 2 N) solutions at time intervals between 1 and 60 min. After the adsorption of 0.1 g of each sample in 10 mg-P L^{-1} of phosphate solution, the phosphate-loaded samples were filtered and dried at 373 K for 24 h. The dried samples were subsequently dispersed in 50 mL of each NaOH solution and shaken at 150 rpm. The phosphate concentration in the supernatants was measured as previously described in Section 2.4. The reusability of the adsorbent was examined by reusing the desorbed adsorbent in a seven-cycle adsorption-desorption experiment and measuring the adsorption performance at the end of each cycle. In each re-adsorption experiment, the sample was dried at 373 K for 24 h prior to the next adsorption. The desorption efficiency (%) was calculated using Equation (2):

$$\%Desorption = \frac{CV}{qm} \times 100 \quad (2)$$

where C is the phosphate concentration (mg L^{-1}) after the desorption process, V is the volume of solution (L), q is the amount of phosphate adsorbed before the desorption process (mg-P g^{-1}), and m is the weight of adsorbent (g).

3. Results and discussion

3.1. Effect of the Zr molar ratio and calcination

Fig. 1 shows the phosphate adsorption ability of the LDH, am-Zr, and the composites both before and after calcination at 573 K. The composites are denoted as Zr(x)/LDH, where x stands for the Zr/Fe molar ratio in the LDH. Calcination caused a significant increase in the phosphate adsorption of the LDH. This was due to the surface adsorption and memory effect (layered structure reconstruction) phenomena in the calcined LDH, while in the uncalcined LDH, most of the phosphate adsorption was only caused by anion exchange [23]. The addition of am-Zr to the LDH matrix in the calcined samples markedly decreased the adsorption capacity. The calcination process crystallized am-Zr to tetragonal ZrO_2 by eliminating the hydroxyl groups that were involved in the adsorption of phosphate as active sites, thus resulting in a significant reduction in phosphate adsorption.

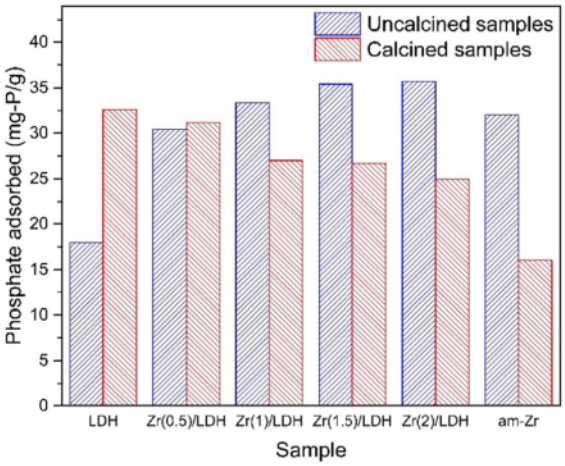

Fig. 1. Phosphate adsorption on LDH, composites, and am-Zr, before and after calcination. (Phosphate concentration: 10 mg-P L^{-1}; Dosage: 0.01 g; Volume: 100 mL; T = ~298 K; pH = 7; t = 24 h).

The introduction of am-Zr in the LDH matrix in the uncalcined samples increased the adsorption capacity as the Zr content increased. In particular, a significant increase in the adsorption capacity occurred as the Zr/Fe molar ratio increased from 0 to 1.5 (from 30.40 mg-P g^{-1} to 35.40 mg-P g^{-1}); however, only a slight increase was observed (to 35.70 mg-P g^{-1}) when the molar ratio was further increased to 2. The composites, except Zr(0.5)/LDH, had much higher adsorption capacities than the LDH (17.99 mg-P g^{-1}) and am-Zr (32.00 mg-P g^{-1}) samples individually. By eliminating the calcination process during the synthesis, the energy consumption of the adsorbent production in the real application can be reduced. Based on this result, the Zr(1.5)/LDH sample was chosen for the following adsorption study, and the term 'composite' is used hereafter to refer specifically to this sample.

3.2. Characterization

The XRD patterns of the uncalcined LDH, am-Zr, composites are illustrated in Fig. 2a. A broad halo around 20–40° of 2θ was observed in am-Zr, which is the typical pattern of amorphous ZrO_2 [20]. The uncalcined LDH exhibited sharp peaks at 2θ of 11.6°, 23.14°, 34.24°, 38.46°, 45.64°, 59.64°, and 60.92°, which correlated with planes (003), (006), (009), (015), (018), (110), and (113) of LDH, respectively [24]. These typical peaks of LDH were also observed in the composites. The lattice parameters c and a of the LDH, which are related to the distance between two neighboring LDH layers and mean cation–cation space, respectively, were calculated using $c = d_{003} + 2d_{006} + 3d_{009}$ and $a = 2d_{110}$ [25]. These parameters were approximately the same between the LDH (c = 23.16 Å and a = 3.08 Å) and the Zr (1.5)/LDH composite (c = 23.20 Å and a = 3.1 Å), thus indicating that the LDH layers were not modified by Zr atoms. In addition, the broad halo of the am-Zr was also

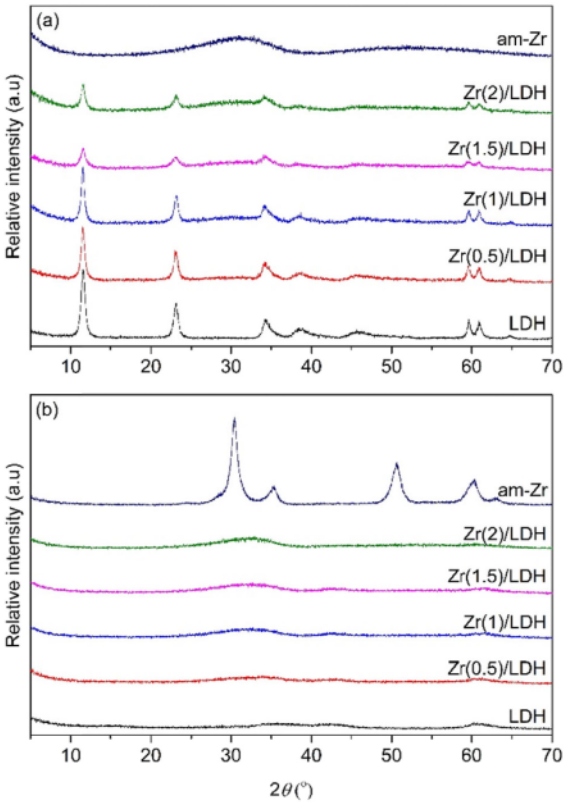

Fig. 2. X-ray powder diffraction patterns of LDH, composites, and am-Zr (a) before calcination, and (b) after calcination.

observed in all of the composites, which indicates that they were the combination of the LDH and am-Zr with no other observed phase. With a lowering of the crystallinity, the adsorption capacity of the composite increased. This signifies that the lowering of the crystallinity corresponded to an increased specific surface area of the composite and an increased amount of hydroxyl groups that acted as active sites [26].

Fig. 2b displays the XRD patterns of samples after calcination at 573 K for 3 h. The am-Zr showed the typical diffraction peaks for tetragonal ZrO_2. However, none of the composites exhibited diffraction peaks for crystalline ZrO_2, thus indicating that ZrO_2 had just started to be crystallized and had a very small tetragonal crystal, which was due to the interference of the LDH structure that collapsed during the calcination process. The patterns for the LDH and composite indicate that the layered structure of the LDH completely collapsed due to the removal of structural water and carbonate anions from the interlayer.

The FTIR spectra of the LDH, composite, and am-Zr samples before calcination in the range of 4000–600 cm^{-1} is shown in Fig. 3a. The OH stretching vibration and LDH interlayer carbonate regions can be found in this region. The intense and broad absorption band centered at around ~3430 cm^{-1} and the band at ~1640 cm^{-1} in all spectra could be attributed to the O–H stretching and bending vibrations caused by hydroxyl groups and physically adsorbed water molecules in the samples, respectively [27]. By comparing the FTIR spectrum of the composite with that of LDH and am-Zr, the bands of the Zr–OH bending vibration were observed at around ~1353 cm^{-1} and ~1565 cm^{-1}, and the band indicating CO_3^{2-} antisymmetric stretching in the interlayer was detected at ~1358 cm^{-1} [28,29].

The lattice vibrations for all samples can be observed in the range of 550–350 cm^{-1} in the FTIR spectra as shown in Fig. 3b. All the bands marked for the LDH reference sample in Fig. 3b represent the bending and stretching vibration of M–O, M–O–M, and O–M–O (M = Mg and Fe) [30–36]. The as-prepared am-Zr sample shows strong absorption bands ~380 cm^{-1} and ~389 cm^{-1} which are indicative for amorphous zirconia [37,38]. Moreover, the tetragonal zirconia (*t*-ZrO_2) bands [37, 39–44] are also found in the am-Zr sample as shown in Fig. 3b, which demonstrate that the nucleation of the metastable *t*-ZrO_2 phase occurred at a few favored points inside the amorphous phase of the am-Zr sample during synthesis. This was predictable since the amorphous zirconium hydroxide has a similar structure with *t*-ZrO_2, and consequently it promotes the crystallization of *t*-ZrO_2 nanocomposite from amorphous structure [45]. All the observed bands in am-Zr and LDH samples are found in the spectra of the composite sample, which signifies that the composite comprises the two primary components, i.e. am-Zr and MgFe-LDH.

The SEM images of the LDH, am-Zr, and composite are presented in Fig. 4a–c. The image of the LDH shows the formation of a platelet-like layered structure, which is characteristic of LDH materials, while the image of am-Zr appears to show nanosized particles agglomerated to a coral-like shape. The micrograph of the as-prepared composite reveals

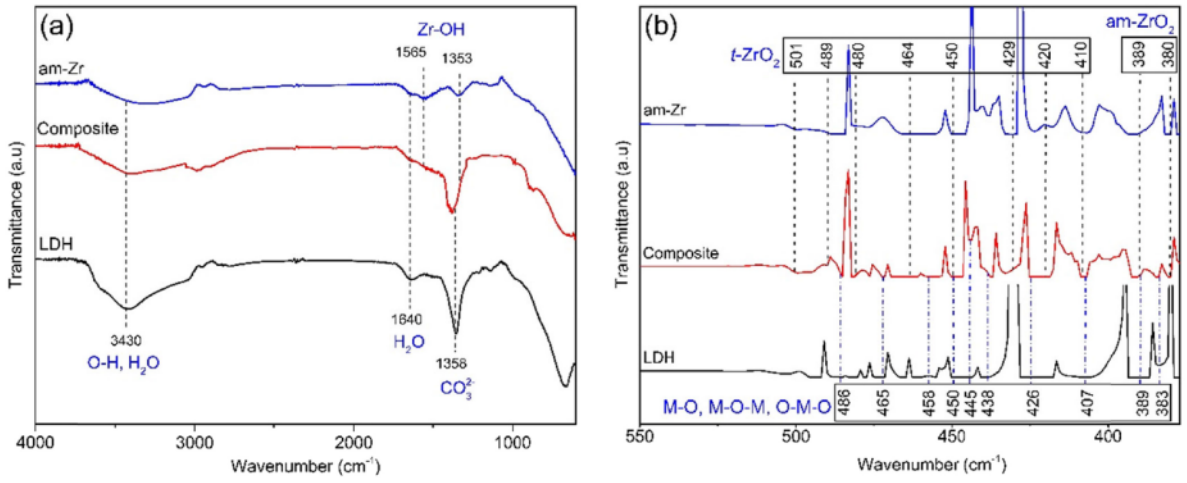

Fig. 3. FTIR spectra of LDH, composite (Zr (1.5)/LDH), and am-Zr before calcination in the range of (a) 4000–600 cm^{-1}, and (b) 550–350 cm^{-1}.

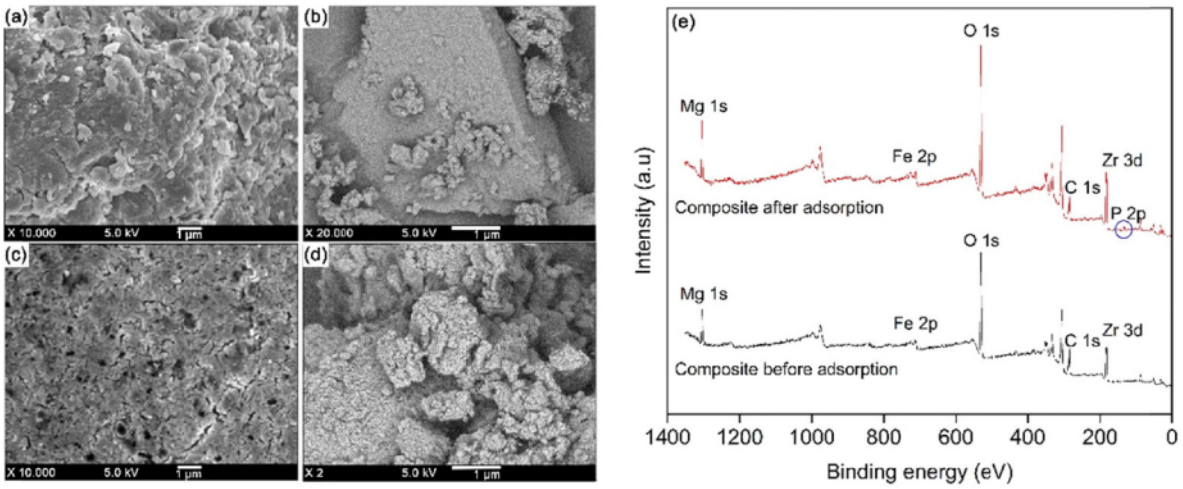

Fig. 4. Scanning electron micrographs of (a) LDH, (b) am-Zr, (c) composite before adsorption and (d) composite after adsorption, and (e) XPS spectra of composite before and after phosphate adsorption.

that the platelet-like structure of the LDH was demolished and broke into smaller nanoparticles with many pores. This combination suppressed the growth of the crystal size and reduced the agglomeration of ultrafine sized ZrO_2. The morphology of the composite after adsorption (Fig. 4d) was changed by the formation of a phosphate substance layer on its surface. From the typical XPS spectra shown in Fig. 4e, the adsorption of phosphate onto the composite surface was confirmed by the appearance of the P2p peak at 134.08 eV after adsorption [46].

3.3. Effect of solution pH

The initial pH dependence graph of phosphate adsorption on the adsorbents is displayed in Fig. 5. The composite and am-Zr exhibited a high phosphate adsorption capacity in very acidic conditions (pH $\leq$ 3), while the adsorption ability of the LDH decreased sharply, which was possibly due to the potential dissolution of Fe and Mg in the LDH at very low pH [47]. The composite could maintain its adsorption ability at pH 2, which was mainly due to the high chemical inertness of ZrO_2 even though the LDH could not preserve its structure at such low pH.

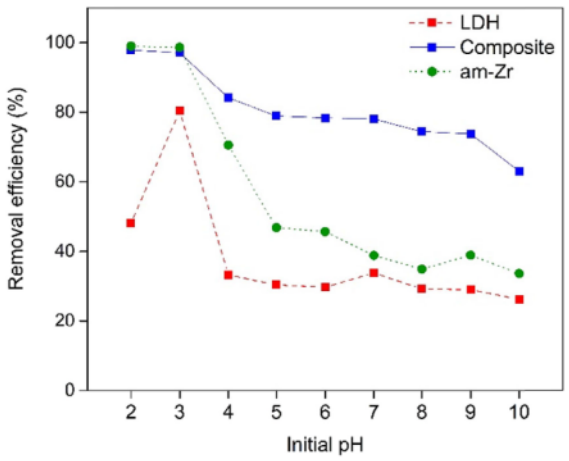

Fig. 5. Effect of initial pH on phosphate adsorption. (Phosphate concentration: 3 mg-P L^{-1}; Dosage: 0.01 g; Volume: 100 mL; T = ~298 K; t = 24 h).

The high phosphate adsorption at low pH was primarily caused by the positively charged adsorbent surface due to protonated hydroxyl groups (OH_2^+), which strongly attracted phosphate anions [48]. On the other hand, the decreased removal efficiency at high pH was attributable to the adsorbent surface, which gradually became more negative due to the increased OH^- ions at higher pH. This led to a higher competition with phosphate ions for binding sites on the surface [49]. Moreover, $H_2PO_4^-$ exists at low pH (2.1–7.2) and is more easily adsorbed on hydrated metal oxides than HPO_4^{2-} that exists at pH 7.2–12.36, thus resulting in a lower adsorption capacity at high pH [50].

The composite showed the highest adsorption over a wide initial pH range of 4–10, thereby indicating that adsorption on the composite was less dependent on the surface charge in comparison to the LDH and am-Zr. The am-Zr on the surface of the LDH likely increased the number of active sites and surface area, which minimized the competition of OH^- ions at high pH. The Lewis acid-base reaction was involved in adsorption under alkaline conditions and was intensified at high pH [46]. The active sites of the adsorbent acted as the Lewis acid, especially Zr atoms that have empty d-orbitals, whereas phosphate anions acted as the Lewis base and donated electrons to form a bond. This result implied that the composite has a wide applicable scope of the pH ranging from 2 to 10, which is suitable for practical utilization, considering that some adsorbents are susceptible to a wide pH range and become a serious problem for wastewater treatment applications that require a long contact time.

3.4. Effect of competing anions

Some anions, such as chloride (Cl^-), nitrate (NO_3^-), sulfate (SO_4^{2-}), and bicarbonate (HCO_3^-), exist along with phosphate ions in waterbodies and wastewater and compete for adsorption sites on adsorbents. The phosphate removal efficiency in some ion solutions was measured to examine the selectivity of phosphate adsorption on the composite. The results are shown in Fig. 6, which illustrates that the coexistence of Cl^-, NO_3^-, and SO_4^{2-} ions had no significant effect on phosphate adsorption, whereas the presence of HCO_3^- considerably decreased the removal efficiency. The HCO_3^- ion at a high concentration (high ratio of CO_3/PO_4) and pH > 7 has been found to generate a highly competitive effect with phosphate [51], whereby HCO_3^- also forms inner-sphere complexation with metal hydroxide surfaces [52]. The strong pentacyclic complex formed between Zr_4^+ and HCO_3^- in the surface of the composite greatly inhibited the adsorption of phosphate on the composite [53]. Moreover, the addition of HCO_3^- would be expected to raise the original solution pH

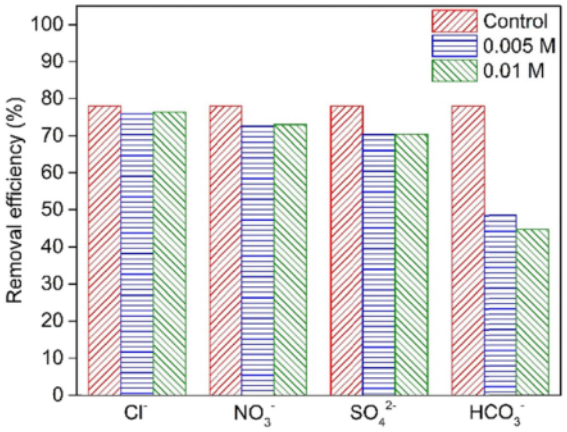

Fig. 6. Effect of common competing anions Cl^-, NO_3^-, SO_4^{2-}, and HCO_3^- on the phosphate removal efficiency. (Phosphate concentration: 3 mg-P L^{-1}; Dosage: 0.01 g; Volume: 100 mL; T = ~298 K; t = 24 h).

to a basic condition which would, in turn, also decrease adsorption capacity. The results indicate that the composite is unsuitable for remediating phosphate from wastewater with a high HCO_3^- concentration.

3.5. Adsorption kinetics

The phosphate adsorption kinetics of the synthesized LDH, composite, and am-Zr are presented in Fig. 7a. A rapid phosphate adsorption onto the composite was observed within the initial 6 h, which then became slower until reaching equilibrium. This adsorption rate was faster than that of am-Zr, which became slower and reached equilibrium after 9 h. The LDH reached equilibrium for ~3 h, but the adsorption capacity was markedly lower than that of the other samples.

To investigate the phosphate adsorption characteristics of the composite, the adsorption kinetics were analyzed using pseudo-first-order and pseudo-second-order models. These models are given by Equations (3) and (4), respectively:

$$\ln(q_e - q_t) = \ln(q_e) - k_1 t \quad (3)$$

$$\frac{t}{q_t} = \frac{1}{k_2 q_e^2} + \frac{1}{q_e} t \quad (4)$$

where q_e and q_t (mg g^{-1}) are the amount of adsorbed phosphate at equilibrium and time t, respectively; k_1 (h^{-1}) and k_2 (g mg^{-1}·h^{-1}) are the rate constant of the pseudo-first-order model and pseudo-second-order model, respectively.

The linear regressions of the pseudo-first-order and pseudo-second-order models are presented in Fig. 7b and c, respectively, and the detailed parametric data are shown in Table 1. The obtained correlation coefficient (R^2) of the pseudo-second-order model was higher than that of the pseudo-first-order model. The experimental value of q_e (36.13 mg-P g^{-1}) obtained from the pseudo-second-order model was close to the calculated value of q_c (36.90 mg g^{-1}). This indicates that the phosphate adsorption process by the am-Zr/LDH composite followed the pseudo-second-order model and chemisorption took control of the adsorption [54].

3.6. Adsorption isotherm

To understand the type of phosphate adsorption onto the composite, the adsorption isotherm was calculated using Langmuir, Freundlich, Temkin, and Dubinin–Radushkevich (D-R) isotherm models which are defined by Equations (5)–(8) respectively:

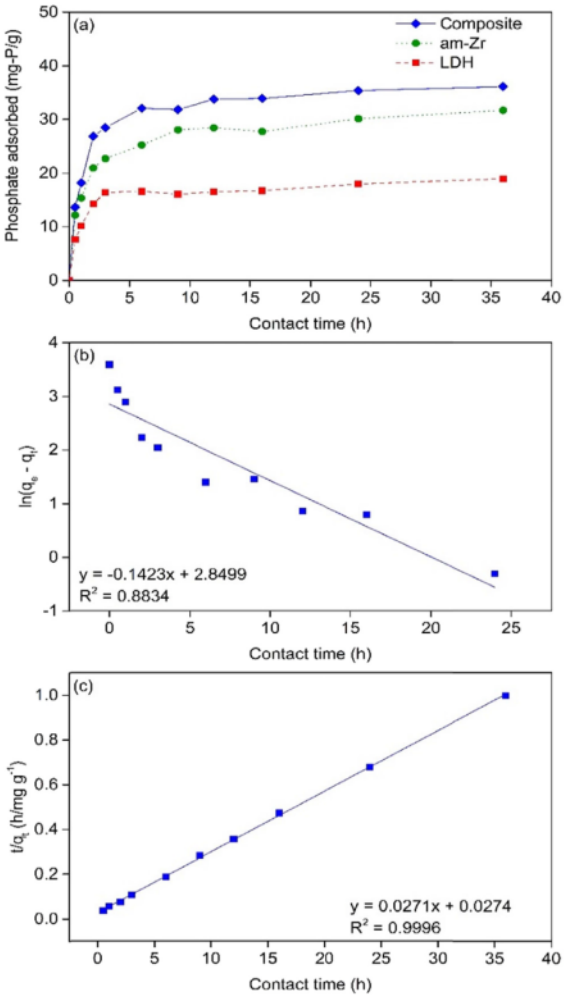

Fig. 7. The plots of: (a) phosphate adsorption capacity of LDH, composite, and am-Zr vs. contact time, (b) pseudo-first-order model of composite, and (c) pseudo-second-order model of composite. (Phosphate concentration: 10 mg-P L^{-1}; Dosage: 0.01 g; Volume: 100 mL; T = ~298 K; pH = 7).

Table 1
Kinetic model parameters for phosphate adsorption by am-Zr/MgFe-LDH composite.

Kinetics model	Parameter	Value
Pseudo-first-order	q_e (mg-P g^{-1})	36.13
	q_c (mg g^{-1})	17.29
	k_1 (h^{-1})	0.3277
	R^2	0.8834
Pseudo-second-order	q_e (mg-P g^{-1})	36.13
	q_c (mg g^{-1})	36.90
	k_2 (g $mg^{-1}h^{-1}$)	0.0268
	R^2	0.9996

$$q_e = \frac{q_m k_l C_e}{1 + k_l C_e} \quad (5)$$

$$q_e = k_f C_e^{1/n} \quad (6)$$

$$q_e = \frac{RT}{bt} \ln(k_t C_e) \quad (7)$$

$$q_e = q_m e^{-[RT \ln(1+1/C_e)]^2 / 2E^2} \quad (8)$$

where C_e (mg-P L^{-1}) is the phosphate equilibrium concentration; q_e (mg-P g^{-1}) is the equilibrium adsorption capacity of the adsorbent; q_m (mg g^{-1}) is the theoretical maximum adsorption capacity of the adsorbent; k_l(L mg^{-1}) is the Langmuir adsorption constant associated with the adsorption energy; k_f (mg g^{-1}) is the Freundlich adsorption constant associated with the adsorption capacity; n is a constant related to adsorption intensity or surface heterogeneity; k_t (L g^{-1}) and b_t (J mol^{-1}) are an equilibrium binding constant and a constant related to the heat of adsorption, respectively; E (kJ mol^{-1}) is the mean free energy of adsorption; R is the universal gas constant (8.314 J K^{-1} mol^{-1}); and T (K) is the absolute temperature.

As shown in Fig. 8, the amount of phosphate adsorbed increased by increasing the initial concentration of the phosphate solution and the surrounding temperature. This was due to the increased collision probability and frequency between phosphate ions and composite active sites. The non-linear fitting plots of adsorption using the Langmuir, Freundlich, Temkin, and D-R equations are shown in Fig. 8a-d, and the relative parameters of the models are summarized in Table 2. The R^2 values of the Freundlich model (0.9688–0.9984) were greater than those of the other isotherm models for all observed temperatures. This indicates that the Freundlich model was the best model to describe the adsorption of phosphate onto the am-Zr/LDH composite. This suggests

Table 2
Isotherm relative parameters for phosphate adsorption by am-Zr/MgFe-LDH composite.

Isotherm	Isotherm constant	Temperature		
		290 K	307 K	324 K
Langmuir	k_l (L mg^{-1})	0.062	0.243	0.189
	q_m (mg g^{-1})	66.08	58.59	64.49
	R^2	0.9113	0.8960	0.9568
Freundlich	k_f (L g^{-1})	11.07	20.56	18.59
	$1/n$	0.39	0.27	0.32
	R^2	0.9688	0.9984	0.9865
Temkin	k_t (L g^{-1})	22.90	28.16	11.00
	b_t (J mol^{-1})	409.43	347.22	297.33
	R^2	0.8285	0.9387	0.9407
D-R	E (kJ mol^{-1})	4.53	14.30	11.21
	q_m (mg g^{-1})	44.56	47.94	51.14
	R^2	0.8449	0.7704	0.8500

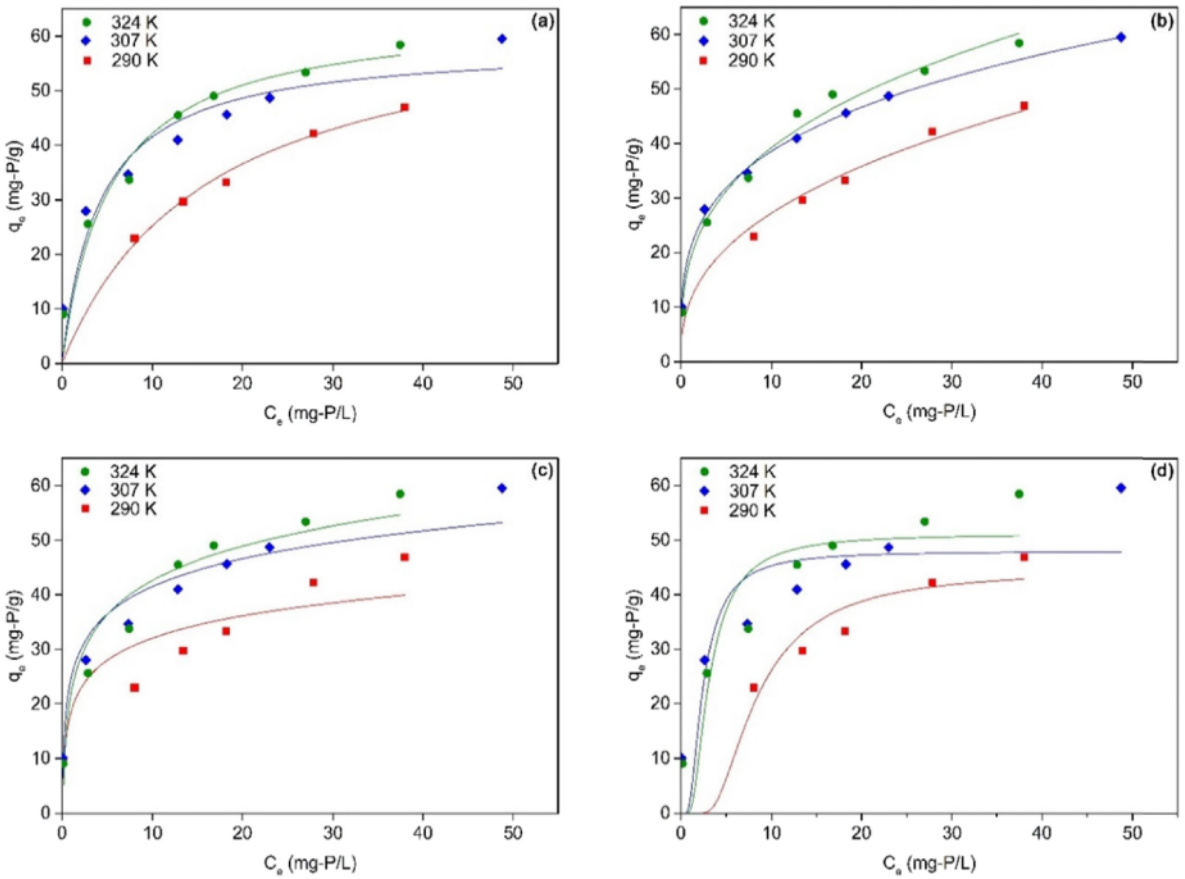

Fig. 8. The non-linear fitting plots of adsorption using the (a) Langmuir, (b) Freundlich, (c) Temkin, and (d) D-R isotherm equations at different treatment temperatures. (Dosage: 0.01 g; Volume: 100 mL; pH = 7; t = 24 h).

that adsorption might have taken place on the surface containing heterogeneous binding sites with different energies, and that adsorption was generated in multilayers on the surface [3,55]. This type of adsorption involves both physical and chemical adsorption [56]. The values of $1/n$ were lower than 0.4, which signified that the adsorption of phosphate onto the composite was essentially favorable.

3.7. Adsorption thermodynamics

The thermodynamic parameters of phosphate adsorption can be calculated from the adsorption isotherm at different temperatures by using Equations (9)–(11):

$$k_d = \frac{q_e}{C_e} \tag{9}$$

$$\Delta G^0 = -RT \ln k_d \tag{10}$$

$$\ln k_d = \frac{\Delta S^0}{R} - \frac{\Delta H^0}{RT} \tag{11}$$

where $k_d$is the distribution coefficient, ΔG^0 (kJ mol^{-1}) is the change of Gibbs energy, and ΔS^0 (kJ mol^{-1} K^{-1}) and ΔH^0 (kJ mol^{-1}) are the change of entropy and enthalpy, respectively. The values of ΔS^0 and ΔH^0 were determined by the plot of ln k_d and $1/T$, where the intercept and the slope of the plot correspond to $\Delta S^0/R$ and $\Delta H^0/R$, respectively.

According to Equations (9)–(11), the thermodynamic parameters were determined from the slope of ln K_d and T^{-1} (Fig. 9). The detailed thermodynamic parameter values are listed in Table 3. The calculated ΔG^0 values were negative, which indicates that the adsorption at all observed temperatures occurred spontaneously. This value decreased with increased temperature, thus indicating that adsorption was more feasible at higher temperatures. The positive value of ΔH^0 reveals that the adsorption process was endothermic. Furthermore, the positive value of ΔS^0 suggests increasing randomness at the solid-solution interface during the adsorption process.

3.8. Phosphate desorption and adsorbent reusability

The recycling performance of the composite was highly affected by phosphate desorption from the composite. Fig. 10a shows the results of the phosphate desorption in NaOH solutions of different concentrations and shaking times, whereby the desorption percentage increased

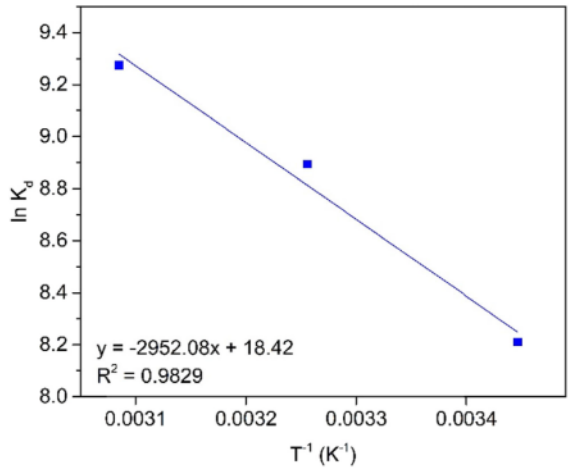

Fig. 9. The plot of the relationship between ln K_d and T^{-1} for the calculation of thermodynamic parameters of phosphate adsorption.

Table 3
Thermodynamic parameters for phosphate adsorption by am-Zr/LDH composite.

Temperature (K)	k_d	ΔG^0 (kJ mol^{-1})	ΔH^0 (kJ mol^{-1})	ΔS^0 (kJ mol^{-1})
290	3679.46	−19.81	24.54	0.1532
307	7282.72	−22.71		
324	10648.85	−24.99		

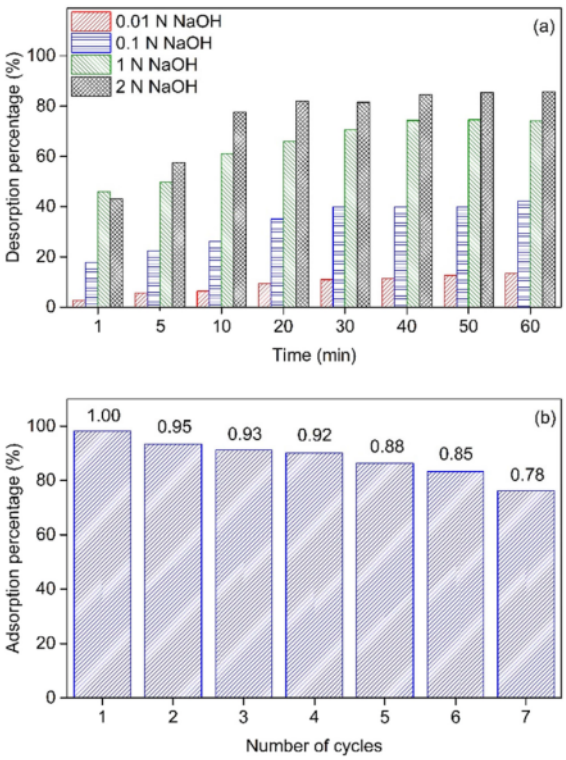

Fig. 10. (a) Phosphate desorption by different concentrations of NaOH solution, and (b) the reusability of composite for phosphate adsorption with desorption solution of 1 N of NaOH (the numbers above the bar are adsorption retain ratio of phosphate adsorption by the composite).

remarkably from 0.1 N to 1 N of NaOH. The optimum desorption of 87.37% was achieved at 2 N of NaOH solution for 40 min desorption time. This optimum desorption time was applied for the adsorbent reusability experiments. Despite the fact that 2 N of NaOH yielded higher desorption than did 1 N, the increase in the desorption was insignificant in comparison to that from 0.1 N to 1 N; hence, 1 N of NaOH was used in the reusability experiments to reduce costs.

Fig. 10b displays the reusability of the composite during seven cycles. After the first cycle, the composite retained 95% of the adsorption ability of the fresh composite. Subsequently, its adsorption ability gradually declined continuously to 78% after the seventh regeneration cycle. The decreasing adsorption ability of the composite reflects the decreasing availability of binding sites on the composite surface after each previous adsorption. The results of the reusability study demonstrated that the composite can hold its removal efficiency at approximately 92% after 4 cycles, emphasizing the practicality and stability of the composite in adsorbent reusability and phosphorus recovery.

4. Conclusions

The am-Zr/MgFe-LDH composite was successfully prepared and used for phosphate removal from aqueous solutions. The XRD analysis showed that the modification of Zr on the LDH layers was eliminated by a two-staged synthesis, which confirmed that the synthesized adsorbent was purely composite. The uncalcined composite with a Zr/Fe ratio of 1.5 at pH 7 had a phosphate adsorption capacity of 35.40 mg-P g^{-1}, which was higher than the uncalcined LDH (17.99 mg-P g^{-1}) and am-Zr (32.00 mg-P g^{-1}). It was also much higher than the calcined samples, which demonstrated that the requirement of calcination in the LDH for phosphate adsorption could be eliminated as a means of reducing energy consumption. The adsorption ability of the composite was considerably stable over a wide pH range and significantly increased at pH $\leq$ 3, which is suitable for practical application. However, this composite may not be applicable to wastewater that contains a high HCO_3^- concentration. On the other hand, this study elucidates the effect of ZrO_2 on the adsorption ability of composites at low pH, as well as the adsorption kinetics and thermodynamics of the adsorbent which was previously unexplained. The regeneration study showed that the synthesized composite is a potential adsorbent for phosphate removal and recovery from water. Ongoing research aims to explain the adsorption mechanism of phosphate on the composite surface and will also test the composite using real wastewater to validate our experimental findings.

CRediT authorship contribution statement

Atin Nuryadin: Conceptualization, Methodology, Formal analysis, Investigation, Data curation, Writing – original draft, Visualization. **Tsuyoshi Imai:** Conceptualization, Methodology, Resources, Writing – review & editing, Supervision, Project administration, Funding acquisition. **Ariyo Kanno:** Conceptualization, Methodology, Writing – review & editing. **Koichi Yamamoto:** Conceptualization, Methodology, Writing – review & editing. **Masahiko Sekine:** Conceptualization, Methodology, Writing – review & editing. **Takaya Higuchi:** Conceptualization, Methodology, Writing – review & editing.

Declaration of competing interest

The authors declare that they have no known competing financial interests or personal relationships that could have appeared to influence the work reported in this paper.

Acknowledgments

The first author gratefully acknowledges the support of the Indonesian Ministry of Research, Technology, and Higher Education (RISTEK-DIKTI), as well as the Project Implementation Unit (PIU) of the Islamic Development Bank (IsDB) 4in1 Project of Mulawarman University for providing the scholarship. The authors would also like to thank Prof. Tasuma Suzuki for assistance with FTIR analysis and Editage (www.editage.com) for English language editing.

References

[1] Y. Deng, T. Zhang, B.K. Sharma, H. Nie, Optimization and mechanism studies on cell disruption and phosphorus recovery from microalgae with magnesium modified hydrochar in assisted hydrothermal system, Sci. Total Environ. 646 (2019) 1140–1154, https://doi.org/10.1016/j.scitotenv.2018.07.369.

[2] M. Le Moal, C. Gascuel-Odoux, A. Ménesguen, Y. Souchon, C. Étrillard, A. Levain, F. Moatar, A. Pannard, P. Souchu, A. Lefebvre, G. Pinay, Eutrophication: a new wine in an old bottle? Sci. Total Environ. 651 (2019) 1–11, https://doi.org/10.1016/j.scitotenv.2018.09.139.

[3] Y. Hu, Y. Du, G. Nie, T. Zhu, Z. Ding, H. Wang, L. Zhang, Selective and efficient sequestration of phosphate from waters using reusable nano-Zr(IV) oxide impregnated agricultural residue anion exchanger, Sci. Total Environ. 700 (2020) 134999, https://doi.org/10.1016/j.scitotenv.2019.134999.

[4] X. Huang, X. Liao, B. Shi, Adsorption removal of phosphate in industrial wastewater by using metal-loaded skin split waste, J. Hazard Mater. 166 (2009) 1261–1265, https://doi.org/10.1016/j.jhazmat.2008.12.045.

[5] W. Huang, Y. Zhang, D. Li, Adsorptive removal of phosphate from water using mesoporous materials: a review, J. Environ. Manag. 193 (2017) 470–482, https://doi.org/10.1016/j.jenvman.2017.02.030.

[6] K. Zhou, B. Wu, L. Su, W. Xin, X. Chai, Enhanced phosphate removal using nanostructured hydrated ferric-zirconium binary oxide confined in a polymeric anion exchanger, Chem. Eng. J. 345 (2018) 640–647, https://doi.org/10.1016/j.cej.2018.01.091.

[7] Y. Makita, A. Sonoda, Y. Sugiura, A. Ogata, C. Suh, J. Lee, K. Ooi, Phosphorus removal from model wastewater using lanthanum hydroxide microcapsules with poly(vinyl chloride) shells, Separ. Purif. Technol. 241 (2020) 116707, https://doi.org/10.1016/j.seppur.2020.116707.

[8] S. Daneshgar, A. Callegari, A.G. Capodaglio, D. Vaccari, The potential phosphorus crisis: resource conservation and possible escape technologies: a review, Resources 7 (2) (2018) 37, https://doi.org/10.3390/resources7020037.

[9] H. Qiu, W. Ni, H. Zhang, K. Chen, J. Yu, Fabrication and evaluation of a regenerable HFO-doped agricultural waste for enhanced adsorption affinity towards phosphate, Sci. Total Environ. 703 (2020) 135493, https://doi.org/10.1016/j.scitotenv.2019.135493.

[10] H. Hatami, A. Fotovat, A. Halajnia, Comparison of adsorption and desorption of phosphate on synthesized Zn-Al LDH by two methods in a simulated soil solution, Appl. Clay Sci. 152 (2018) 333–341, https://doi.org/10.1016/j.clay.2017.11.032.

[11] X. Sun, T. Imai, M. Sekine, T. Higuchi, K. Yamamoto, K. AkagiI, Adsorption of phosphate by calcinated Mg-Fe layered double hydroxide, J. Water Environ. Technol. 11 (2) (2013) 111–120, https://doi.org/10.2965/jwet.2013.111.

[12] S. Iftekhar, M.E. Küçük, V. Srivastava, E. Repo, M. Sillanpää, Application of zinc-aluminium layered double hydroxides for adsorptive removal of phosphate and sulfate: equilibrium, kinetic and thermodynamic, Chemosphere 209 (2018) 470–479, https://doi.org/10.1016/j.chemosphere.2018.06.115.

[13] W. Wang, H. Zhang, L. Zhang, H. Wan, S. Zheng, Z. Xu, Adsorptive removal of phosphate by magnetic Fe_3O_4@C@ZrO_2, Colloids Surfaces A Physicochem. Eng. Asp. 469 (2015) 100–106, https://doi.org/10.1016/j.colsurfa.2015.01.002.

[14] F. Long, J.L. Gong, G.M. Zeng, L. Chen, X.Y. Wang, J.H. Deng, Q.Y. Niu, H. Y. Zhang, X.R. Zhang, Removal of phosphate from aqueous solution by magnetic Fe-Zr binary oxide, Chem. Eng. J. 171 (2) (2011) 448–455, https://doi.org/10.1016/j.cej.2011.03.102.

[15] X. Luo, X. Wang, S. Bao, X. Liu, W. Zhang, T. Fang, Adsorption of phosphate in water using one-step synthesized zirconium-loaded reduced graphene oxide, Sci. Rep. 6 (2016) 39108, https://doi.org/10.1038/srep39108.

[16] J. Wang, Y. Liu, P. Hu, R. Huang, Adsorption of phosphate from aqueous solution by Zr(IV)-crosslinked quaternized chitosan/bentonite composite, Environ. Prog. Sustain. Energy 37 (1) (2018) 267–275, https://doi.org/10.1002/ep.12667.

[17] S. Mallakpour, M. Hatami, An effective, low-cost and recyclable bio-adsorbent having amino acid intercalated LDH@Fe_3O_4/PVA magnetic nanocomposites for removal of methyl orange from aqueous solution, Appl. Clay Sci. 174 (2019) 127–137, https://doi.org/10.1016/j.clay.2019.03.026.

[18] R. Chitrakar, S. Tezuka, J. Hosokawa, Y. Makita, A. Sonoda, K. Ooi, T. Hirotsu, Uptake properties of phosphate on a novel Zr-modified MgFe-LDH(CO_3), J. Colloid Interface Sci. 349 (1) (2010) 314–320, https://doi.org/10.1016/j.jcis.2010.05.068.

[19] H. Miyauchi, T. Yamamoto, R. Chitrakar, Y. Makita, Z. Wang, J. Kawai, T. Hirotsu, Phosphate adsorption site on zirconium ion modified MgAl-layered double hydroxides, Top. Catal. 52 (2009) 714–723, https://doi.org/10.1007/s11244-009-9209-1.

[20] R. Chitrakar, S. Tezuka, A. Sonoda, K. Sakane, K. Ooi, T. Hirotsu, Synthesis and phosphate uptake behavior of Zr^{4+} incorporated MgAl-layered double hydroxides, J. Colloid Interface Sci. 313 (1) (2007) 53–63, https://doi.org/10.1016/j.jcis.2007.04.004.

[21] S. Velu, D.P. Sabde, N. Shah, S. Sivasanker, New hydrotalcite-like anionic clays containing Zr^{4+} in the Layers: synthesis and physicochemical properties, Chem. Mater. 10 (11) (1998) 3451–3458, https://doi.org/10.1021/cm980185x.

[22] D. Tichit, N. Das, B. Coq, R. Durand, Preparation of Zr-containing layered double hydroxides and characterization of the acido-basic properties of their mixed oxides, Chem. Mater. 14 (4) (2002) 1530–1538, https://doi.org/10.1021/cm011125l.

[23] R. Elmoubarki, F.Z. Mahjoubi, A. Elhalil, H. Tounsadi, M. Abdennouri, M. Sadiq, S. Qourzal, A. Zouhri, N. Barka, Ni/Fe and Mg/Fe layered double hydroxides and their calcined derivatives: preparation, characterization and application on textile dyes removal, J. Mater. Res. Technol. 6 (3) (2017) 271–283, https://doi.org/10.1016/J.JMRT.2016.09.007.

[24] T.-T.H. Nguyen, X.-T.T. Nguyen, C.Q. Nguyen, P.H. Tran, Porous metal oxides derived from Cu–Al layered double hydroxide as an efficient heterogeneous catalyst for the Friedel–Crafts alkylation of indoles with benzaldehydes under microwave irradiation, Heliyon 4 (11) (2018), e00966, https://doi.org/10.1016/j.heliyon.2018.e00966.

[25] E. Heraldy, K.D. Nugrahaningtyas, Heriyanto, X-ray diffraction analysis on post treatment of Ca-Mg-Al-layered double hydroxide slurry, IOP Conf. Ser. Mater. Sci. Eng. 176 (2017) 012020, https://doi.org/10.1088/1757-899x/176/1/012020.

[26] Y. Seida, Y. Nakano, Removal of phosphate in dissolution-coagulation process of layered double hydroxide, J. Chem. Eng. Jpn. 34 (7) (2001) 906–911, https://doi.org/10.1252/jcej.34.906.

[27] Y. Su, H. Cui, Q. Li, S. Gao, J.K. Shang, Strong adsorption of phosphate by amorphous zirconium oxide nanoparticles, Water Res. 47 (14) (2013) 5018–5026, https://doi.org/10.1016/j.watres.2013.05.044.

[28] X. Dou, D. Mohan, C.U. Pittman, S. Yang, Remediating fluoride from water using hydrous zirconium oxide, Chem. Eng. J. 198–199 (2012) 236–245, https://doi.org/10.1016/j.cej.2012.05.084.
[29] V.R. Magri, A. Duarte, G.F. Perotti, V.R.L. Constantino, Investigation of thermal behavior of layered double hydroxides intercalated with carboxymethylcellulose aiming bio-carbon based nanocomposites, ChemEngineering 3 (2) (2019) 55, https://doi.org/10.3390/chemengineering3020055.
[30] P. Samoila, C. Cojocaru, I. Cretescu, C.D. Stan, V. Nica, L. Sacarescu, V. Harabagiu, Nanosized spinel ferrites synthesized by sol-gel autocombustion for optimized removal of azo dye from aqueous solution, J. Nanomater. 2015 (2015) 713802, https://doi.org/10.1155/2015/713802.
[31] B.P. Jacob, A. Kumar, R.P. Pant, S. Singh, E.M. Mohammed, Influence of preparation method on structural and magnetic properties of nickel ferrite nanoparticles, Bull. Mater. Sci. 34 (2011) 1345–1350, https://doi.org/10.1007/s12034-011-0326-7.
[32] K. Rybka, J. Matusik, A. Kuligiewicz, T. Leiviskä, G. Cempura, Surface chemistry and structure evaluation of Mg/Al and Mg/Fe LDH derived from magnesite and dolomite in comparison to LDH obtained from chemicals, Appl. Surf. Sci. 538 (2021) 147923, https://doi.org/10.1016/j.apsusc.2020.147923.
[33] T.N. Brusentsova, R.E. Peale, D. Maukonen, G.E. Harlow, J.S. Boesenberg, D. Ebel, Far infrared spectroscopy of carbonate minerals, Am. Mineral. 95 (2010) 1515–1522, https://doi.org/10.2138/am.2010.3380.
[34] P.A. Schroeder, Infrared spectroscopy in clay science, in: A.C. Rule, S. Guggenheim (Eds.), Teaching clay science 11, Clay Mineral Society, Aurora, CO, 2002, pp. 182–206. https://doi.org/10.1346/CMS-WLS-11.11.
[35] P. Marzbani, H. Resalati, A. Ghasemian, A. Shakeri, Surface modification of talc particles with phthalimide: study of composite structure and consequences on physical, mechanical, and optical properties of deinked pulp, BioResources 11 (4) (2016) 8720–8738, https://doi.org/10.15376/biores.11.4.8720-8738.
[36] R.C. Zeng, Z.G. Liu, F. Zhang, S.Q. Li, H.Z. Cui, E.H. Han, Corrosion of molybdate intercalated hydrotalcite coating on AZ31 Mg alloy, J. Mater. Chem. A. 2 (2014) 13049–13057, https://doi.org/10.1039/c4ta01341g.
[37] T. Ivanova, A. Harizanova, T. Koutzarova, N. Krins, B. Vertruyen, Electrochromic TiO_2, ZrO_2 and TiO_2-ZrO_2 thin films by dip-coating method, Mater. Sci. Eng. B Solid-State Mater. Adv. Technol. 165 (3) (2009) 212–216, https://doi.org/10.1016/j.mseb.2009.07.013.
[38] H.J. Quah, Z. Hassan, W.F. Lim, Passivation of silicon substrate using two-step grown ternary aluminium doped zirconium oxide, Appl. Surf. Sci. 493 (2019) 411–422, https://doi.org/10.1016/j.apsusc.2019.07.023.
[39] N.S. Hassan, A.A. Jalil, F.F.A. Aziz, A.A. Fauzi, M.S. Azami, N.W.C. Jusoh, Tailoring the silica amount in stabilizing the tetragonal phase of zirconia for enhanced photodegradation of 2-chlorophenol, Top. Catal. 63 (2020) 1145–1156, https://doi.org/10.1007/s11244-020-01274-3.
[40] M. Ranjbar, M. Yousefi, M. Lahooti, A. Malekzadeh, Preparation and characterization of tetragonal zirconium oxide nanocrystals from isophthalic acid-zirconium(IV) nanocomposite as a new precursor, Int. J. Nanosci. Nanotechnol. 8 (4) (2012) 191–196. http://www.ijnnonline.net/article_3891.html.
[41] F. Monte, W. Larsen, J.D. Mackenzie, Stabilization of tetragonal ZrO_2 in ZrO_2-SiO_2 binary oxides, J. Am. Ceram. Soc. 83 (3) (2004) 628–634, https://doi.org/10.1111/j.1151-2916.2000.tb01243.x.
[42] A. Arjun, A. Dharr, T. Raguram, K.S. Rajni, Study of copper doped zirconium dioxide nanoparticles synthesized via sol–gel technique for photocatalytic applications, J. Inorg. Organomet. Polym. Mater. 30 (2020) 4989–4998, https://doi.org/10.1007/s10904-020-01616-4.
[43] W. Li, X. Liu, A. Huang, P.K. Chu, Structure and properties of zirconia (ZrO_2) films fabricated by plasma-assisted cathodic arc deposition, J. Phys. D Appl. Phys. 40 (8) (2007) 2293–2299, https://doi.org/10.1088/0022-3727/40/8/S08.
[44] F. Bollino, E. Armenia, E. Tranquillo, Zirconia/hydroxyapatite composites synthesized via sol-gel: influence of hydroxyapatite content and heating on their biological properties, Materials 10 (7) (2017) 757, https://doi.org/10.3390/ma10070757.
[45] J. Li Vage, K. Doi, C. Maziers, Nature and thermal evolution of amorphous hydrated zirconium oxide, J. Am. Ceram. Soc. 51 (6) (1968) 349–353, https://doi.org/10.1111/j.1151-2916.1968.tb15952.x.
[46] S. Dong, Q. Ji, Y. Wang, H. Liu, J. Qu, Enhanced phosphate removal using zirconium hydroxide encapsulated in quaternized cellulose, J. Environ. Sci. 89 (2020) 102–112, https://doi.org/10.1016/j.jes.2019.10.005.
[47] H. Zhou, Z. Jiang, S. Wei, A new hydrotalcite-like absorbent FeMnMg-LDH and its adsorption capacity for Pb^{2+} ions in water, Appl. Clay Sci. 153 (2018) 29–37, https://doi.org/10.1016/j.clay.2017.11.033.
[48] R. Li, J.J. Wang, B. Zhou, M.K. Awasthi, A. Ali, Z. Zhang, L.A. Gaston, A.H. Lahori, A. Mahar, Enhancing phosphate adsorption by Mg/Al layered double hydroxide functionalized biochar with different Mg/Al ratios, Sci. Total Environ. 559 (2016) 121–129, https://doi.org/10.1016/j.scitotenv.2016.03.151.
[49] K. Dox, M. Everaert, R. Merckx, E. Smolders, Optimization of phosphate recovery from urine by layered double hydroxides, Sci. Total Environ. 682 (2019) 437–446, https://doi.org/10.1016/j.scitotenv.2019.05.181.
[50] J. Li, B. Li, H. Huang, X. Lv, N. Zhao, G. Guo, D. Zhang, Removal of phosphate from aqueous solution by dolomite-modified biochar derived from urban dewatered sewage sludge, Sci. Total Environ. 687 (2019) 460–469, https://doi.org/10.1016/j.scitotenv.2019.05.400.
[51] J.C. Mendez, T. Hiemstra, Carbonate adsorption to ferrihydrite: competitive interaction with phosphate for use in soil systems, ACS Earth Sp. Chem. 3 (1) (2019) 129–141, https://doi.org/10.1021/acsearthspacechem.8b00160.
[52] R.B. Balow, J.G. Lundin, G.C. Daniels, W.O. Gordon, M. McEntee, G.W. Peterson, J. H. Wynne, P.E. Pehrsson, Environmental effects on zirconium hydroxide nanoparticles and chemical warfare agent decomposition: implications of atmospheric water and carbon dioxide, ACS Appl. Mater. Interfaces 9 (45) (2017) 39747–39757, https://doi.org/10.1021/acsami.7b10902.
[53] Q. Dong, S. Shi, Y. Xie, Y. Wang, X. Zhang, X. Wang, S. Guo, L. Zhu, G. Zhang, D. Xu, Preparation of mesoporous zirconia ceramic fibers modified by dual surfactants and their phosphate adsorption characteristics, Ceram. Int. 46 (9) (2020) 14019–14029, https://doi.org/10.1016/j.ceramint.2020.02.201.
[54] W. Gu, X. Li, M. Xing, W. Fang, D. Wu, Removal of phosphate from water by amine-functionalized copper ferrite chelated with La(III), Sci. Total Environ. 619–620 (2018) 42–48, https://doi.org/10.1016/j.scitotenv.2017.11.098, 42–48.
[55] N. Tahir, H.N. Bhatti, M. Iqbal, S. Noreen, Biopolymers composites with peanut hull waste biomass and application for Crystal Violet adsorption, Int. J. Biol. Macromol. 94 (Part A) (2017) 210–220, https://doi.org/10.1016/j.ijbiomac.2016.10.013.
[56] X. Zhang, H. Han, X. Zheng, T. Yu, Y. Chen, Tetracycline-induced effects on the nitrogen transformations in sediments: roles of adsorption behavior and bacterial activity, Sci. Total Environ. 695 (2019) 133811, https://doi.org/10.1016/j.scitotenv.2019.133811.

Phosphate adsorption and desorption on two-stage synthesized amorphous-ZrO2/Mg–Fe layered double hydroxide composite

ORIGINALITY REPORT

9%	5%	4%	0%
SIMILARITY INDEX	INTERNET SOURCES	PUBLICATIONS	STUDENT PAPERS

MATCH ALL SOURCES (ONLY SELECTED SOURCE PRINTED)

6%

★ www.gjesm.net

Internet Source

Exclude quotes	On	Exclude matches	< 3%
Exclude bibliography	On		